Phase Transition of Thermally Treated Polyhedral Nano Nickel Oxide with Reduced Band Gap

Peeyush Phogat[1]*, *Shreya*[1], *Ranjana Jha*[1] *and Sukhvir Singh*[1]

[1] Research Systems for Energy Systems, Department of Physics, Netaji Subhas University of Technology, Dwarka, New Delhi, INDIA

Abstract. Nickel oxide (NiO) is a semiconducting material which exhibits a unique electronic structure. Because of its distinctive electronic properties, NiO stands as an intriguing candidate for various applications in optoelectronics, photo catalysis, and energy devices such as solar cells. In the present work efforts have been made to tailor the band gap of NiO. A simple co-precipitation method followed by heat treatment is utilized to synthesize the material. Prior to heat treatment, x-ray diffraction study of the as synthesized material showed the presence of nickel hydroxide [$Ni(OH)_2$]. On calcination for one hour at 1000^oC, a single phase NiO was revealed. After heat treatment it was noticed that the particle size was found to be increased. The absorption spectra of [$Ni(OH)_2$] and NiO were recorded using UV-Vis spectroscopy method. Using Tauc plot a band gap of 4.2 eV and 1.8 eV for $Ni(OH)_2$ and NiO was observed respectively. It is observed that a significant decrease in band gap of NiO was noticed. Surface morphological study was carried out by using FESEM, which revealed the transformation of sheet like structures of [$Ni(OH)_2$] to polyhedral shaped NiO on calcination. The presence of nickel and oxygen was confirmed by the energy dispersive spectrometry analysis.

1 Introduction

Substantial progress has been achieved in the expansion of renewable and sustainable energy sources during the last decade. The advancement of renewable energy sources such as solar cells and electrochemical technologies such as capacitors/supercapacitors and batteries (lithium ion) is critical for fostering a cleaner world [1–3]. To advance these technologies, a primary requirement is the study of material properties. Extensive research has been conducted on anode materials for solar cell applications, whether involving II–VI semiconductors or transition metals in general [4, 5]. Nevertheless, there remains a need to explore and investigate novel cathode materials for solar cell applications.
Nickel oxide (NiO) is a well-known cathode material with a band gap of 3.5 to 4 eV [6]. The unique characteristics of nickel oxide nanoparticles make this material highly promising for a variety of applications like energy storage, optoelectronics, etc. [7–9].

* Corresponding author: peeyush.phogat@gmail.com

NiO has gained a prominence in the field of solar cells primarily due to its tunable band gap, which enables the material to absorb more sunlight and convert it efficiently into electric energy. NiO-based solar cells hold particular appeal due to their potential cost-effectiveness and sustainability. While NiO is inherently a wide band gap material, the reduction in its band gap can present intriguing and innovative avenues in material science and its applications. Conventionally, the wide band gap of NiO has limited its utility in optoelectronic and energy-related applications [10]. However, through the techniques presented in this manuscript, namely nanostructuring, and thermal treatment, the authors have successfully engineered NiO with a reduced band gap. This reduction in the band gap holds immense promise, facilitating improved light absorption, enhanced charge transport, and expanded opportunities in photovoltaics. Increased absorption of light results in improved photovoltaic performance, enhancing sensitivity in photodetectors, wider range of emission spectra, will provide better performance in infrared applications and facilitates tuning electronic properties and carrier transport properties.

An effort has been undertaken in the present research work to synthesize NiO with a reduced band gap. Co-precipitation technique was used to easily complete the synthesis in one step. The phase of the nickel oxide and nickel hydroxide materials was identified using the X-ray powder diffraction (XRD) method. The crystallite size and microstrain were determined using the Debyes-Sherrer equation and the Williamson Hall (W-H) plot, respectively. UV-Vis Spectroscopy was utilized to investigate the optical properties and band gap of the materials. The morphological traits associated with them were studied using a field emission scanning electron microscope (FESEM). Elemental compositional analysis was performed utilizing energy dispersive spectrometer (EDS) as an attachment of FESEM.

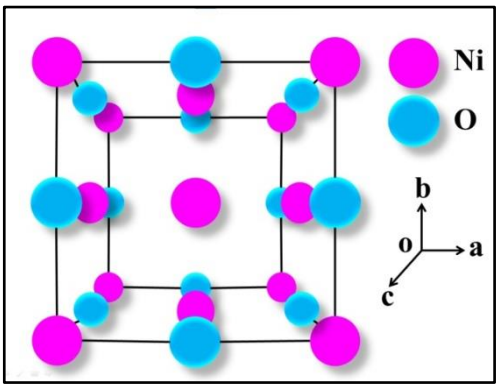

Fig. 1. 3D model of cubic NiO.

2 Experimental Procedure

2.1 Chemicals Used

15Mega-Ohm resistivity distilled water and pure alcohol were used for washing and synthesis. DI water was used to make all of the solutions. Table-1 lists the other compounds that were utilized.

Table 1. Chemicals Used.

Chemicals Name	Company

Nickel (II) nitrate hexahydrate [$Ni(NO_3)_2 .6H_2O$]	M/s Thomas Baker
Sodium Hydroxide (NaOH)	M/s Thomas Baker

2.2 Synthesis

Nickel nitrate hexahydrate was diffused in DI water to prepare a 0.96 M solution. Concurrently, a 1.25 M solution of sodium hydroxide was prepared. Magnetic stirrers were used to mix both solutions for one hour. The addition of the NaOH solution to the $Ni(NO_3)_2 .6H_2O$ solution for $Ni(OH)_2$ formation was carried out using a burette, and a controlled dropwise addition was crucial for optimal nanoparticles development. The subsequent blend was further diffused for four hours at room temperature. Subsequently, the liquid was then subjected to filtration. Filtration and washing steps were repeated three times, involving rinsing with distilled water and then with 100% ethanol. Afterward, the sample was dried in a vacuum oven at pressure of 600 mm of Hg and a temperature of 120 °C. Once dried, it was allowed to cool overnight before being finely powdered. The fine powder was finally calcinated in oxygen atmosphere at 1000°C for 1 hour.

2.3 Characterization Details

To understand the structure and phase of the material, the fine powder of the as synthesized sample was studied with an X-Ray Diffractometer (make:Panalytical and model X'pert PRO). Copper (Cu) K(alpha)-radiation (=1.5406A^o) was used to record the x-ray diffraction pattern. For the morphological and elemental compositional analysis, a FESEM (model:7610FPlus, make:JEOL) with an EDS attachment was employed. The optical response of the as produced material was measured using a SHIMADZU UV-2600i UV Vis spectrometer.

3 Results and Discussion

3.1 X-Ray Diffraction

The x-ray diffraction pattern for the as synthesized powder samples was recorded over a 2θ range of 10^o to 80^o. The diffraction peaks were analyzed and indexed to the standard JCPDS file: ***00-001-1047,*** which exhibited a good match with nickel hydroxide [$Ni(OH)_2$]. The as synthesized $Ni(OH)_2$ displayed a hexagonal crystal system, with identified peaks corresponding to the hkl planes (100), (101), (102), (110) and (111). $Ni(OH)_2$ showed low crystallinity with high noise, specifically in the region of 10^o to 30^o as shown in figure-2(a). However, following the thermal treatment, XRD measurement was again performed for calcinated sample in the same range of 2θ as mentioned above. The observed pattern demonstrate high crystallinity with well resolved and distinct peaks, which were subsequently analyzed and indexed to JCPDS file: ***01-078-0423***. The calcinated sample showed a strong correlation with nickel oxide (NiO) and exhibited a cubic crystal system when compared with standard JCPDS file ***01-078-0423***. The reflection peaks corresponded to the hkl planes (111), (200), (220), (311) and (222) belongs to the cubic structure having polycrystalline nature as shown in figure-2(b).

The JCPDS file indicated the crystal structure of NiO to be in a space group Fm3m. The "Fm3m" crystal system refers to the face-centered cubic (fcc) crystal system. In an fcc crystal system, each lattice point is shared by eight adjacent unit cells, which results in a highly symmetric and dense packing of atoms or ions. This crystal system is commonly encountered in various materials, including metals like aluminium, copper, and gold, as well as some ionic compounds. Figure-1 depicts the cubic crystal system of NiO.

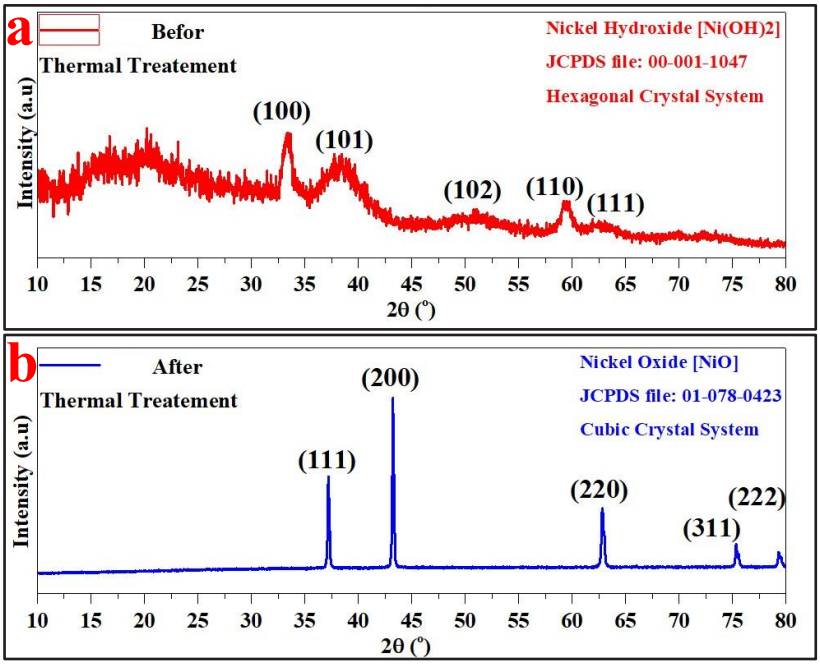

Fig. 2.(a) XRD pattern for as synthesized $Ni(OH)_2$, **(b)** XRD pattern for calcined $Ni(OH)_2$ revealing the formation of single phase cubic NiO with polycrystalline nature.

3.2 Lattice Parameters, Crystallite Size and Strain

Nickel nitrate Crystallite size refers to the size of individual crystal grain within a material. This unique property of any nanomaterial is determined through a well-known equation known as Debye Scherrer formula given in equation-1 as [11],

$$D = \frac{K\lambda}{\beta \mathrm{Cos}\theta} \quad (1)$$

Here, D associates to the crystal grain size (crystallite size), K is a constant of 0.9 known as Scherrer constant, λ is the wavelength of x-ray source given by 0.154nm, β is full with at half of maxima (FWHM) and θ is half the position XRD pattern. The calculation of crystallite size was performed by taking an average of all the analyzed peaks. The resulting crystallite size for $Ni(OH)_2$ and NiO was approximately 12 nm and 78 nm respectively. The crystallite size for $Ni(OH)_2$ lies in quantum dot region, which signifies quantum confinement and existence of quantum electronical states [12]. Whereas after the thermal treatment of $Ni(OH)_2$, the crystallite size increases due to several factors such as recrystallization, annealing, energy redistribution and grain growth.

However, Debye-Scherrer analysis is based on the assumption that there is no strain present in the material. To verify the presence of strain, lattice parameters were calculated. $Ni(OH)_2$

and NiO showed an hexagonal and cubic crystal system respectively. Hence to calculate the deviation in lattice parameters the formula presented in equation-2(a&b) has been used [13, 14],

$$\frac{1}{d^2} = \frac{4}{3}\left(\frac{h^2+k^2+hk}{a^2}\right) + \frac{l^2}{c^2} \quad \text{(for Hexagonal)} \tag{2a}$$

$$\frac{1}{d^2} = \frac{h^2}{a^2} + \frac{k^2}{b^2} + \frac{l^2}{c^2} \quad \text{(for Cubic)} \tag{2b}$$

The interplaner spacing is d, the miller indices are h,k,l, and the lattice parameters are a,b,c. Table-2 shows the comparison of lattice parameters between JCPDS file and calculated values.

Table 2. Lattice Parameters.

Parameters	**As synthesized Ni(OH)2**	**$Ni(OH)_2$ in JCPDS file: *00-001-1047***	**As synthesized NiO**	**NiO in JCPDS file: *01-078-0423***
a (Å)	3.08	3.07	4.18	4.17
b (Å)	3.08	3.07	4.18	4.17
c (Å)	4.71	4.60	4.18	4.17

The table above illustrate that the calculated value deviates from the standard once due to the presence of micro strain present in the materials. To calculate the strain a well-known method known as Williamson Hall plot was applied. Williamson Hall plot (W-H plot) states that broadening of XRD peaks not only from crystallite size but also from strain. The W-H equation is given as equation-3 [1, 15, 16],

$$\beta_T Cos\theta = (\varepsilon \times 4Sin\theta) + \frac{K\lambda}{D} \tag{3}$$

Here in equation-3, ε is the micro strain present in the as synthesized material. Plotting the graph between 4Sinθ versus βCosθ and comparing the value of slope depicted in figure-3(a&b) reveals the micro strain to be -0.0087 and -1.02×10^{-4} for $Ni(OH)_2$ and NiO respectively. The negative strain present in the material reveals compression present in the material. The compression in $Ni(OH)_2$ causes the confinement. The comparison of intercept revealed the crystallite size of approximately 6 nm and 66 nm for $Ni(OH)_2$ and NiO respectively. In the Debye-Scherrer equation, the assumption was made that there was no strain present in the material. However, when calculating the Williamson-Hall Plot, microstrain was taken into account, leading to differences in the inferred particle size. The variability in the Williamson-Hall plot was attributed to the measured Full Width Half Maxima (FWHMs) resulting from instrumental broadening. Also, due to the presence of strain, the crystallite size of the material could not be confined to a single value; instead, it always existed within a range. Table-3 presents all the values calculated from the Debye-Scherrer equation and the W-H plot.

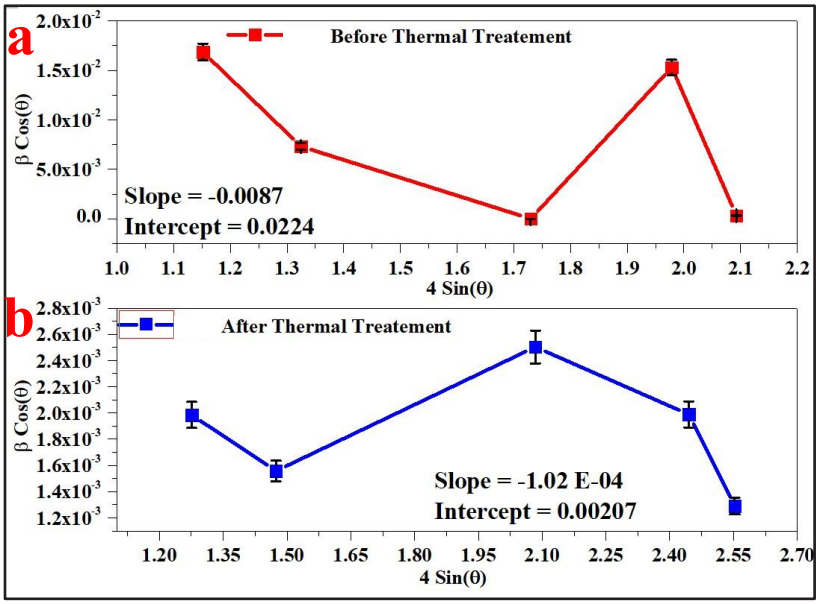

Fig. 3.(a) Williamson Hall plot for $Ni(OH)_2$, **(b)** Williamson Hall plot for NiO.

Table 3. Crystallite Size and strain.

Parameters	Debye Scherrer Size	Williamson Hall Size	Williamson Hall Strain	W-H Plot Slope	W-H Plot Intercept
$Ni(OH)_2$	12 nm	6 nm	-0.0087	-0.0087	0.0224
NiO	78 nm	66 nm	-1.02×10^{-4}	-1.02×10^{-4}	0..00207

3.3 UV-Vis Spectroscopy

The optical response of as synthesized powder was recorded in a range of 190 nm to 850 nm using diffusion reflectance spectroscopy (DRS). The absorbance curve reveals that $Ni(OH)_2$ exhibited absorbance solely in the UV region, specifically between 193 nm to 235 nm with small absorbance at 390 nm and from 665 nm to 671 nm (as shown in figure-4(a)). The maximum absorbance was observed at a wavelength of 231 nm. However, after the thermal treatment, the absorbance peaks exhibit a red shift towards visible region. The as synthesized NiO showed absorbance from 191 nm to 850 nm, covering the entire absorption spectrum, indicating that the material is well suited for solar cell applications. The maximum absorbance for NiO was observed at 722 nm, 724 nm and 725 nm as shown in figure-4(b). The material exhibits an intriguing absorbance phenomenon, demonstrating absorbance in both the UV and the entire visible spectrum. To obtain the band gap of both samples, Tauc's plot was plotted as shown in figure-4(c&d). Tauc plot was obtained using equation-4, given as [17],

$$\alpha h\upsilon = A[h\upsilon - E_g]^{\frac{1}{n}} \quad (4)$$

Where α is absorbance coefficient, hυ is the input energy of photon, A is the constant for energy, Eg is the bandgap, and n is the exponent reflecting the type of the transition. The band gap for $Ni(OH)_2$ and NiO was computed using the aforementioned equation and establish to be 4.2 eV and 1.8 eV, respectively. NiO shows a band gap of 3.5 eV to 4 eV, however due to quantum confinement in $Ni(OH)_2$ the transition from larger band gap to smaller band gap has caused an extreme reduction in NiO band gap.

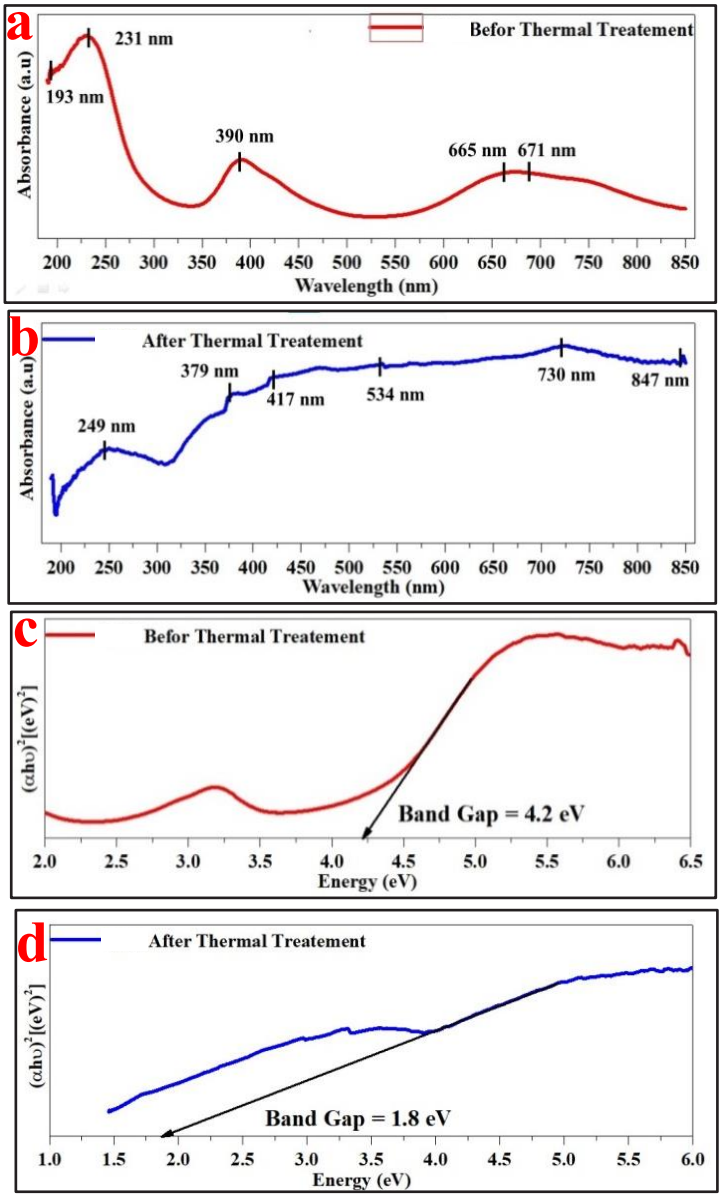

Fig. 4.(a) Absorption spectra for $Ni(OH)_2$, **(b)** absorption spectra for NiO, **(c)** Tauc's plot for $Ni(OH)_2$, **(d)** Tauc's plot for NiO revealing band gap.

3.4 Refractive Index

Refractive index (RI) plays an important role in solar cell application of the sample. The RI can affect how efficiently light interacts with the layer of solar cell. When the refractive indices of the material and the medium are matched, more light can penetrate the medium and reach the absorbing layer, increasing the productivity of solar cell. For calculating the refractive index of the samples the equation (5) has been taken in consideration [18-20],

$$\frac{n^2-1}{n^2+2} = 1 - \sqrt{\frac{E_g}{20}} \quad (5)$$

Here, n represents the refractive index, whereas E_g is the respective band gap of $Ni(OH)_2$ and NiO (i.e., 4.2 eV and 1.8 eV). Using the values of band gap the calculated refractive index came out to be 2.18 and 2.82 for $Ni(OH)_2$ and NiO respectively. In general, materials with refractive indices greater than 1.0 indicate that light travels more slowly in that medium compared to a vacuum. The higher the refractive index, the more a material can bend light and more suitable for solar applications. Table 4. Summarizes the max. absorbance, band gap and refractive index of $Ni(OH)_2$ and NiO.

Table 4. Band Gaps and Refractive Index.

Parameters	Max Absorbance	Band Gap	Refractive Index
Ni(OH)2	231 nm	4.2 eV	2.18
NiO	722-725 nm	1.8 eV	2.82

3.5 FESEM

Figure 5(a) shows FESEM image of nickel hydroxide recorded at suitable magnifications. Nanosheets stacked together are clearly seen in the SEM image along with some scattered particles. Thermal treatment of $Ni(OH)_2$ underwent morphological changes throughout the calcination process, which led to an increase in particle size as depicted in figure 5(b) having polyhedral shape attached together. Average size of these polyhedral particles are found to be of the order of 500 nm. As indicated in fig. 5(c&d), elemental compositional analysis of the relevant sections revealed the existence of just oxygen and nickel

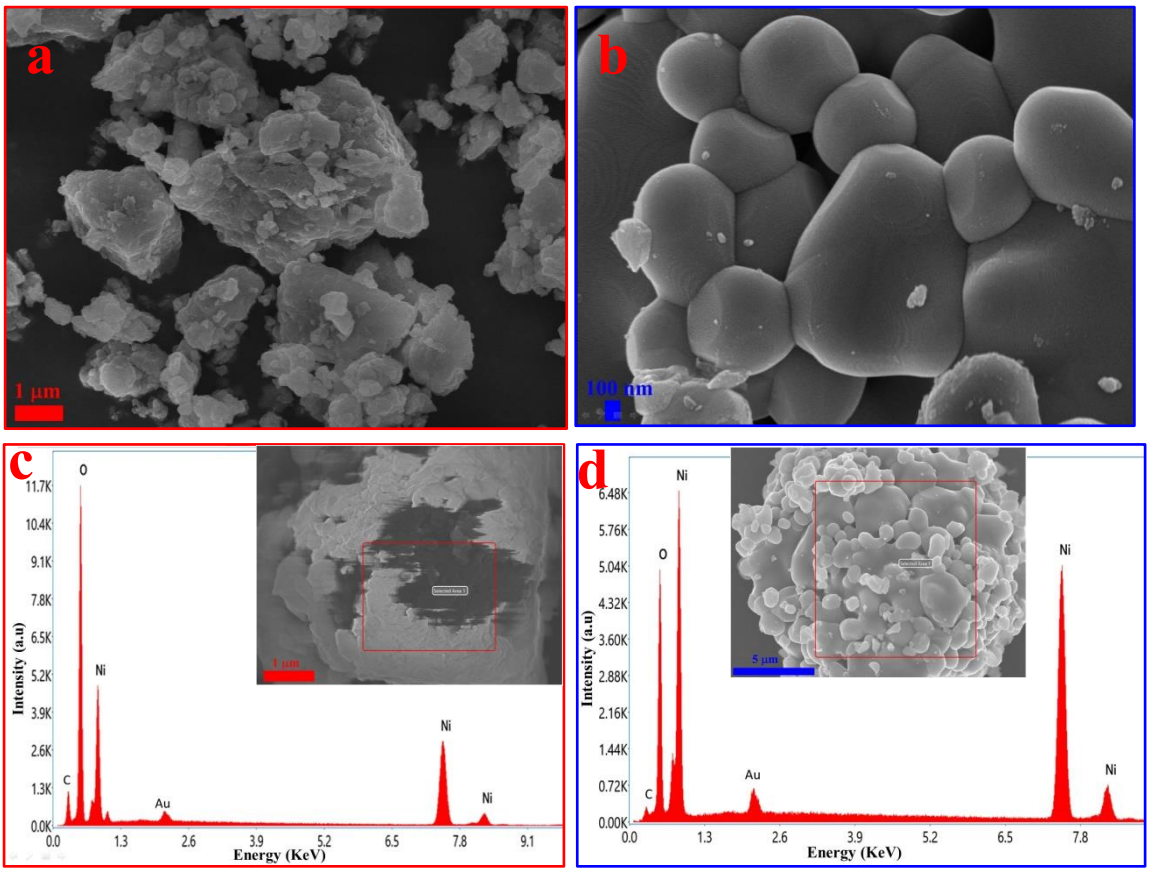

Fig. 5.(a) FESEM images for $Ni(OH)_2$, **(b)** FESEM images for NiO, **(c)** EDX spectra for $Ni(OH)_2$ with inserted selected area, **(d)** EDX spectra for NiO with inserted selected area.

4 Conclusion

The present work is devoted to the synthesis of reduced band gap NiO particles for suitability in solar cell applications. The NiO was synthesized using facile co-precipitation synthesis route. Structural study confirms the presence of both $Ni(OH)_2$ before thermal treatment and NiO phase after thermal treatment. Detailed morphological analysis depicts the stacked sheet like morphology for $Ni(OH)_2$ whereas after thermal treatment the morphology shows a round and polyhedral like morphology with significant increase in the particle size. The novelty of the present work is the noteworthy reduction in band gap. $Ni(OH)_2$ showed a large band gap of 4.2 eV which lies in insulating region while NiO showed an extreme reduction in energy band gap with 1.8 eV which is highly suitable for solar cell applications.

The contributors warmly credit Prof. Anand Srivastava, Hon. Vice Chancellor of Netaji Subhas University of Technology, for providing infrastructural resources.
Peeyush Phogat: Conceptualization, Writing - original draft and Formal analysis. Shreya: Formal analysis and software. Ranjana Jha: Supervision. Sukhvir Singh: Supervision, Writing – review & editing.
All data is presented in the mansucript
There are no conflicts of interest among the writers.

References

1 Dipti, P. Phogat, Shreya, D. Kumari, S. Singh, Fabrication of tunable band gap carbon based zinc nanocomposites for enhanced capacitive behaviour, *Phys. Scr.*, **98**, 9, 95030, (2023). doi: 10.1088/1402-4896/acf07b.

2 S. Sharma, P. Phogat, R. Jha, S. Singh, Electrochemical and Optical Properties of Microwave Assisted MoS_2 Nanospheres for Solar Cell Application, **12**, 3, 66–72, (2023). doi: 10.12720/sgce.12.3.66-72.

3 P. PHOGAT, Shreya, R. JHA, S. Singh, Diffusion Controlled Features of Microwave Assisted ZnS/ZnO Nanocomposite with Reduced Band Gap, *ECS J. Solid State Sci. Technol.*, **12**, 3, 034004, (2023). doi: 10.1149/2162-8777/acc426.

4 T. Kumar, Shreya, P. Phogat, V. Sahgal, R. JHA, Surfactant-Mediated Modulation of Morphology and Charge Transfer Dynamics in Tungsten Oxide Nanoparticles, *Phys. Scr.*, **98**, 8, 085936, (2023). doi: 10.1088/1402-4896/ace566.

5 P. Phogat, Shreya, R. Jha, S. Singh, Optical and Microstructural Study of Wide Band Gap ZnO@ZnS Core--Shell Nanorods to be Used as Solar Cell Applications, in *Recent Advances in Mechanical Engineering*, (2023), 419–429.

6 R. Goel, R. Jha, C. Ravikant, Nickel oxide (NiO) nano-triangles with enhanced electrochromic and photovoltaics properties, *Chem. Pap.*, **77**, 5, 2885–2903,(2023). doi: 10.1007/s11696-023-02673-y.

7 R. Goel, R. Jha, C. Ravikant, Solution-processed spin coated multilayer structured nickel oxide thin films for anodic electrochromism, *J. Appl. Electrochem.*, **53**, 4, 713–735, (2023). doi: 10.1007/s10800-022-01807-6.

8 R. Goel, R. Jha, C. Ravikant, Synergistic effect of Urea and Potassium Sulphate during hydrothermal synthesis of NiO nanospheres with reduced crystallite size and enhanced electrical conductivity, *Inorg. Chem. Commun.*, **141**, 109563,(2022). doi: https://doi.org/10.1016/j.inoche.2022.109563.

9 R. Goel, R. Jha, M. Bhushan, R. Bhardwaj, C. Ravikant, Hydrothermally synthesized nickel oxide (NiO) nano petals, *Mater. Today Proc.*, **48**, 687–689, (2022). doi: https://doi.org/10.1016/j.matpr.2021.08.094.

10 R. Goel, R. Jha, C. Ravikant, Investigating the structural, electrochemical, and optical properties of p-type spherical nickel oxide (NiO) nanoparticles, *J. Phys. Chem. Solids*, **144**, 109488, (2020), doi: https://doi.org/10.1016/j.jpcs.2020.109488.

11 Shreya, P. Phogat, R. Jha, S. Singh, Elevated Refractive Index of MoS2 Amorphous Nanoparticles with a Reduced Band Gap Applicable for Optoelectronics BT - Recent Advances in Mechanical Engineering, in *Recent Advances in Mechanical Engineering*, B. Sethuraman, P. Jain, and M. Gupta, Eds. Singapore: Springer Nature Singapore, (2023), 431–439.

12 P. Phogat, Shreya, R. Jha, S. Singh, Impedance Study of Zinc Sulphide Quantum Dots via One Step Green Synthesis, *Mater. Sci. Forum*, **1099**, 119–125, (2023). doi: 10.4028/p-G1CCxq.

13 Shreya, P. Phogat, R. Jha, S. Singh, Microwave-synthesized γ-WO3 nanorods exhibiting high current density and diffusion characteristics, *Transit. Met. Chem.*, **48**, 3, 167–183, (2023), doi: 10.1007/s11243-023-00533-y.

14 P. Phogat, Shreya, R. Jha, S. Singh, Electrochemical analysis of thermally treated two dimensional zinc sulphide hexagonal nano-sheets with reduced band gap, *Phys. Scr.*, **98**, 12, 125962, (2023), doi: 10.1088/1402-4896/ad0d93.

15 Shreya, A. Yadav, R. Khatri, N. Jain, A. Bhandari, N. K. Puri, “Double Zone

Thermal CVD and Plasma Enhanced CVD Systems for Deposition of Films/Coatings with Eminent Conformal Coverage BT - Advances in Manufacturing Technology and Management," in *Advances in Manufacturing Technology and Management*, R. M. Singari, P. K. Jain, and H. Kumar, Eds. Singapore: Springer Nature Singapore, (2023), 273–283.

16 A. Yadav, Shreya, and N. K. Puri, "Preliminary Observations of Synthesized WS2 and Various Synthesis Techniques for Preparation of Nanomaterials," in *Advances in Manufacturing Technology and Management*, Springer Science and Business Media Deutschland GmbH, (2023), 546–556.

17 R. Bhardwaj, R. Jha, M. Bhushan, R. Sharma, Comparative study of the electrochemical properties of mesoporous 1-D and 3-D nano- structured rhombohedral nickel sulfide in alkaline electrolytes, *J. Phys. Chem. Solids*, **144**, 109503, (2020). doi: 10.1016/j.jpcs.2020.109503.

18 M. Bhushan, R. Jha, Surface activity correlations of mesoporous 3-D hierarchical ZnS nanostructures for enhanced photo and electro catalytic performance, *Appl. Surf. Sci.*, **528**, 146988, (2020), doi: 10.1016/j.apsusc.2020.146988.

19 J. Dahiya, P. Phogat, A. Hooda, and S. Khasa, Investigations of Praseodymium doped LiF-ZnO-Bi2O3-B2O3 glass matrix for photonic applications, *AIP Conf. Proc.*, **2995**, 1, 20065, (2024). doi: 10.1063/5.0178197.

20 D. Kumari, Shreya, P. Phogat, Dipti, S. Singh, R. Jha, Enhanced electrochemical behavior of C@CdS Core-Shell heterostructures, *Mater. Sci. Eng. B*, **301**, 117212, (2024), doi: https://doi.org/10.1016/j.mseb.2024.117212.